applied sciences

MDPI

Article

Design and Implementation of Position-Based Repetitive Control Torque Observer for Cogging Torque Compensation in PMSM

Chun-Ju Wu [1], Mi-Ching Tsai [2,*] and Lon-Jay Cheng [1]

[1] Delta Electronics, Inc., Tainan 74144, Taiwan; coryadam830719@gmail.com (C.-J.W.); lonjie.cheng@gmail.com (L.-J.C.)
[2] Department of Mechanical Engineering, National Cheng Kung University, Tainan 70101, Taiwan
* Correspondence: mctsai@mail.ncku.edu.tw; Tel.: +886-6-2757575-62173

Received: 20 November 2019; Accepted: 16 December 2019; Published: 20 December 2019

Featured Application: Low speed control of PM motor drive.

Abstract: In permanent magnet machines, the cogging torque caused by reluctance variations in the air gap may degrade the speed control performance in low speed and will undoubtedly limit its operational range. In order to reduce the cogging torque, this paper proposes a position-based repetitive control observer aiming at cogging torque estimation and further rejection. This new scheme of observer design possesses the capability of repeatedly learning the observed clogging torque in each rotation to achieve higher estimation accuracy. An online/offline feedforward compensation strategy that employs the forgetting factor principle and position-based average generates the cogging torque compensation lookup table learned from the position-based repetitive control observer. To verify the overall control performance of the proposed observed design technique, a hardware in the loop control device is employed, and then an experimental setup with a permanent magnet synchronous motor and its power drive was adopted.

Keywords: PMSM; cogging torque; position-based repetitive control; model-based disturbance observer

1. Introduction

Servo drive systems are widely used from household appliances to industrial automatic facilities. Permanent magnet synchronous motors (PMSMs) especially play a key role in servo drive systems due to their high performance. Permanent magnets in PMSMs are adopted to provide the required air gap flux density with advantages such as high starting torque, high efficiency, and high power density. However, permanent magnets might cause reluctance variations in the air gap as rotation, and hence generate a periodic reluctance torque ripple called "cogging torque", which is a function of rotor position [1]. As a torque disturbance, the cogging torque may degrade the speed control performance in low speed and would undoubtedly limit the operational range of a PMSM.

It can be found from the literature that there are two kinds of methods to reduce the cogging torque effect. The first one comes from the design of the machine itself. By reducing the reluctance variance between the slots and teeth [2,3], or by skewing the rotor and stator to distract reluctance variance [4,5], the cogging torque can be reduced effectively. However, altering the physical structure of a PMSM might be expensive and tedious, or degrade the motor performance. The other well-known approach is using control methods.

As for the control methods, to achieve appropriate torque disturbance rejection, the method for accurate cogging torque estimation is critical. The MRDOB (model reference disturbance observer), originally from the Luenburger observer [6], can achieve flexible and instantaneous estimation. However, the lack of an internal model [7,8] of the cogging torque in the control loop will limit the estimation performance of the observer in practice. From the literature, the PBRC (position-based repetitive controller) (i.e., spatial-based or angle-based) [9] can be employed as an internal model of the cogging torque in observer design. As shown in Figure 1, this paper combines the design of MRDOB and PBRC as a novel speed and torque observer to achieve accurate disturbance estimation. Based on the estimated torque, both online and offline compensation strategies are proposed for the suppression of cogging torque disturbance, which deteriorates the speed control accuracy, especially at low speed. The online compensation strategy is based on real-time spatial lookup table estimation, which is suitable to overcome the problem caused by the dynamic change of permanent magnets, such as predictive maintenance, fault detection, or the measurement of permanent magnets. Whereas, the offline strategy is used for applications in which permanent magnets is assumed to be static, and a fixed spatial lookup table is used to compensate cogging torque directly according to the rotor position.

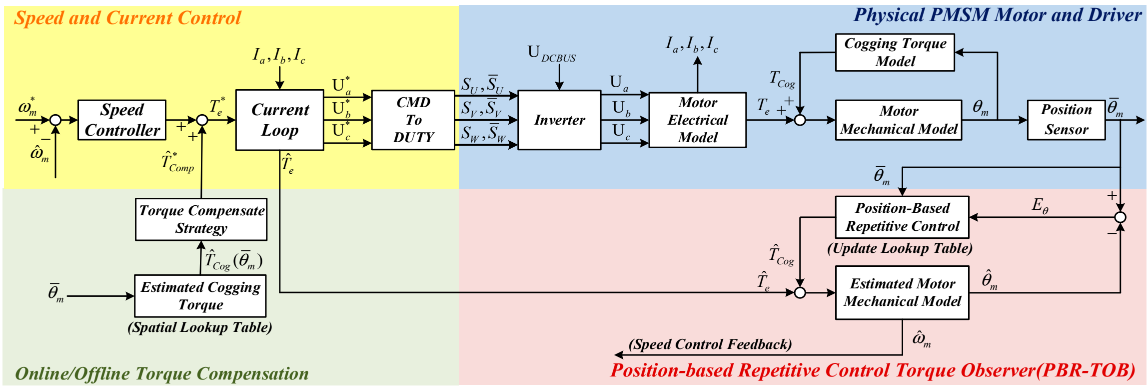

Figure 1. Proposed structure for cogging torque estimation and torque compensation strategy.

To clarify the design concept and implement details, the content of this paper is organized as follows. Section 2 will introduce the detail design and principle of proposed observer. Then, the practical realization process is specified. Two torque compensation structures are proposed: the online torque compensation with a spatial lookup table learning structure and the offline torque compensation structure by a fixed spatial lookup table. In Section 3, a HIL (Hardware-in-the-Loop) experiment is firstly used to evaluate the feasibility of the proposed observer and compensation strategies by an ideal emulation motor model, and afterwards, a practical experiment with real motor and dynamometer is conducted to verify the HIL experiment. Finally, Section 4 concludes the contributions in this paper and issues that needed to be handled in the future.

2. Position-Based Repetitive Torque Observer and Compensation Strategy

2.1. Disturbance Torque Observer

In order to estimate the cogging torque of a PM machine, a classical disturbance torque observer, as shown in Figure 2a, utilizes the input current and the output speed information of the motor. For the case where the observer model is well estimated, i.e., $\hat{J} = J$, $\hat{B} = B$, and $\hat{K}_t = K_t$ the PI controller suppresses the speed error E_ω to approach zero, and the cogging torque $\hat{T}_{Cog}$ can be estimated simultaneously.

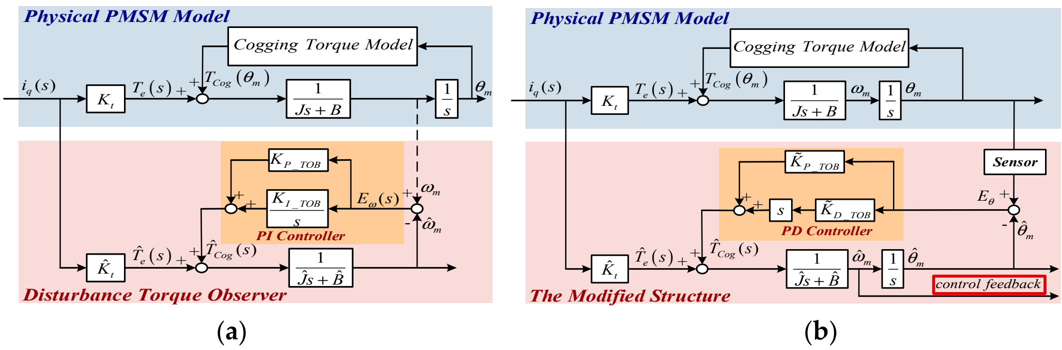

Figure 2. (**a**) Torque disturbance observer; (**b**) Modified structure based on position measurement.

Since the rotor speed information is obtained by a filtered derivation method based on the encoder position data, which might cause delay for the estimated rotor speed and then mislead the results, an alternative observer structure that utilizes the encoder data directly is proposed, as shown in Figure 2b. The output of the modified structure is the motor position, which is compared with the encoder position information directly to estimate the cogging torque. Since the rotor speed is replaced by the rotor position in the modified structure, the PI controller is replaced by the PD controller with gain designed as $\widetilde{K}_{D\_TOB} = K_{P\_TOB}, \widetilde{K}_{P\_TOB} = K_{I\_TOB}$ for the equivalence of these two structures. Another advantage of the proposed structure is that the motor speed information can be obtained directly from the observer as the speed control feedback.

The physical cogging torque model can be represented as given below [10]:

$$T_{Cog}(\theta_m) = \sum_{n=1}^{\infty} C_n \sin(nN_L\theta_m) = \sum_{n=1}^{\infty} C_n \sin(nN_L\omega_m t), \tag{1}$$

where N_L is the least common multiple of the stator slots number and the rotor poles number, and C_n is the amplitude of the n th harmonic. The fundamental frequency of the cogging torque can be expressed as $\omega_{Cog} = N_L\omega_m$. Note that the observer bandwidth ω_{TOB} should be designed to be 10 times higher than the fundamental cogging torque frequency such that

$$\omega_{TOB} \geq 10\left|\omega_{Cog}\right| \tag{2}$$

Correspondingly, the observer bandwidth is 10 times higher than that of the speed control loop such that

$$\omega_{TOB} \geq \left|10 \cdot 2\pi f_\omega\right| \tag{3}$$

If the observer model is well estimated, the transfer function from the cogging torque to its estimation is given by

$$\frac{\hat{T}_{Cog}(s)}{T_{Cog}(\theta_m)} = \frac{(\widetilde{K}_{D\_TOB}s + \widetilde{K}_{P\_TOB})/\hat{J}}{s^2 + (\hat{B} + \widetilde{K}_{D\_TOB})s/\hat{J} + \widetilde{K}_{P\_TOB}/\hat{J}} = H(s) \tag{4}$$

Let the magnitude of $H(s)$ at the bandwidth frequency of ω_{TOB} be described as:

$$\frac{\left|H(j\omega_{TOB})\right|^2}{\left|H(0)\right|^2} = \frac{1}{2} \tag{5}$$

Then,

$$\hat{J}^2\omega_{TOB}^4 - (2\hat{J}\widetilde{K}_{P\_TOB} + \widetilde{K}_{D\_TOB}^2 - 2\hat{B}\widetilde{K}_{D\_TOB} - \hat{B}^2)\omega_{TOB}^2 - \widetilde{K}_{P\_TOB}^2 = 0 \tag{6}$$

Let the zero of $H(s)$ be less than the designed bandwidth and close to the origin such as:

$$s = \frac{-\widetilde{K}_{P\_TOB}}{\widetilde{K}_{D\_TOB}} = -n \cdot \omega_{TOB},\ n << 1 \tag{7}$$

Combining Equations (7) and (8), the observer parameters can be solved as:

$$\begin{cases} \widetilde{K}_{D\_TOB} = \frac{-(2n \cdot \hat{J} \cdot \omega_{TOB} - 2\hat{B}) + \sqrt{(2n \cdot \hat{J} \cdot \omega_{TOB} - 2B)^2 + 4(n^2+1)(\hat{J}^2 \omega_{TOB}^2 + \hat{B}^2)}}{2(n+1)} \\ \widetilde{K}_{P\_TOB} = n\omega_{TOB} \cdot \widetilde{K}_{D\_TOB} \end{cases} \tag{8}$$

For example, consider a system with $\hat{J} = 1 \times 10^{-2}$, $\hat{B} = 1 \times 10^{-3}$ and the observer bandwidth ω_{TOB} to be $100 \times 2\pi$, for $n = 0.1$; then, the resulting parameters from Equations (8) and (9) are $\widetilde{K}_{D\_TOB} = 5.6617$ and $\widetilde{K}_{P\_TOB} = 355.7333$. The Bode plot of $H(s)$ is shown in Figure 3, which approximates to the first-order system.

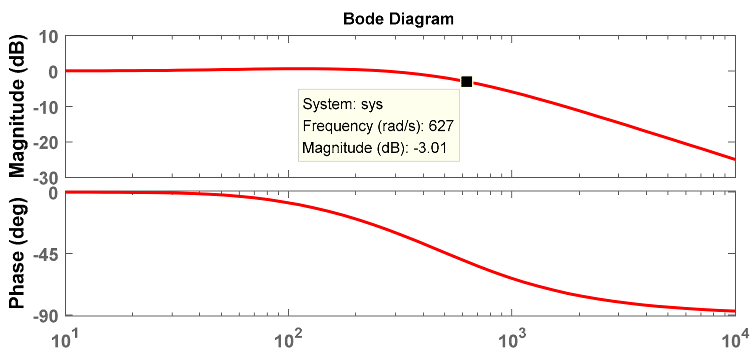

Figure 3. Observer Bode plot for $\hat{J} = 0.01$, $\hat{B} = 0.001$, $\omega_{TOB} = 200\pi$ *and* $n = 0.1$.

Since the cogging torque is periodic, the classical PD or PI controller cannot guarantee that the observer error E_θ in steady state could ever approach zero, which means that the difference between T_{Cog} and $\hat{T}_{Cog}$ will always exist. Therefore, the position-based repetitive controller (PBRC) is employed in the observer design, as shown in Figure 4. Similar to the cogging torque model, the PBRC offers an internal model that learns the cogging torque as a function of the rotor position; in other words, it updates the spatial lookup table iteratively and eventually minimizes the observer error E_θ. In practice, the position-based (PB) delay can be realized by the memory array read/write process, which is triggered by encoder position pulses. The principle and a detailed realization method of PBRC will be addressed in the following sections.

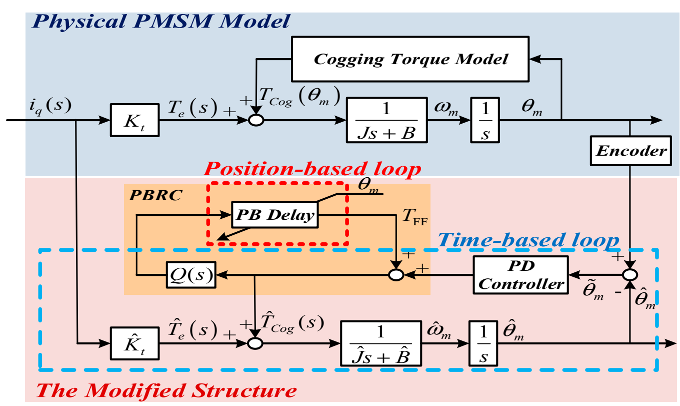

Figure 4. Proposed position-based repetitive control torque observer structure (PBR-TOB).

2.2. Principle of Position-Based Repetitive Controller

The purpose of the repetitive controller (RC) is to track time-based periodic references or reject periodic disturbances. Proposed by Hara [10], the RC is based on an internal model principle (IMP) [7,8]. RC is often used in a control loop to generate an internal model for the controller to cancel out the periodic error caused by periodic references or periodic disturbances. For a periodic signal with period T (sec), the corresponding plug-in type [11] RC is shown in Figure 5a, which can be simplified as Figure 5b. The learning filter $Q(s)$ is a low-pass filter applied to avoid the infinite poles located on imaginary axis, which might cause a stability problem.

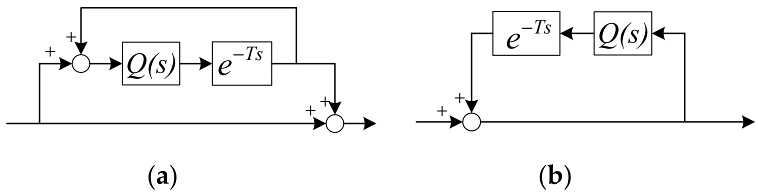

Figure 5. (**a**) Plug-in type repetitive controller (RC); (**b**) Simplified structure.

Since the cogging torque is a position-based periodic signal, as the rotor speed changes, the period changes correspondingly, as shown in Figure 6. An ordinary time-based repetitive controller will fail to track or reject the cogging torque disturbance. The delay index must be changed from time-based dependent to position-based dependent. An alternative structure for the cogging torque is proposed as shown in Figure 7. In other words, the position-based (PB) [12] delay will delay input data for the time needed of a rotor turn (2π).

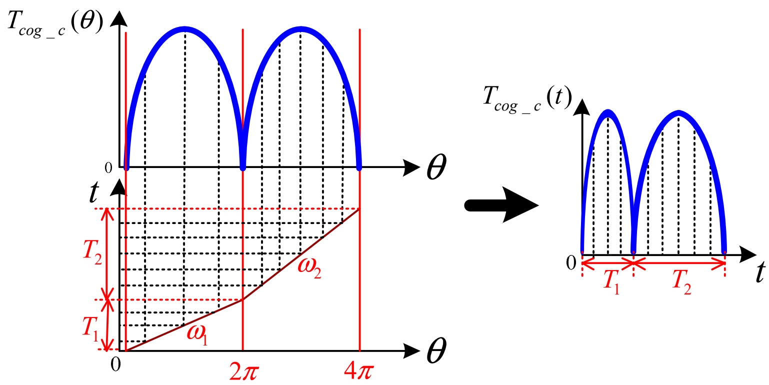

Figure 6. Frequency-varying characteristic of the cogging torque signal.

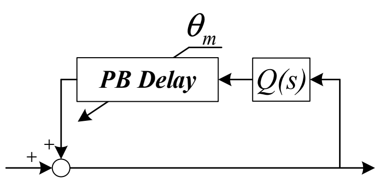

Figure 7. Position-based repetitive controller for the cogging torque signal.

The learning filter $Q(s)$ plays a key role in the trade-off design between torque estimation accuracy and stability of the RC observer. A low-pass filter is given by $Q(s) = \omega_Q/(s + \omega_Q)$ in this paper.

2.3. Realization of PBR-TOB

As shown in Figure 4, the position-based repetitive control torque observer structure (PBR-TOB) structure consists of a torque observer structure (TOB), which is a linear time-based observer (enclosed in blue dashed line), and a PBR, which is a nonlinear position-based delay function (enclosed in red dotted line). To implement the above design, the signal processing flow of the Digital Signal Processor (DSP) includes two sub-flows, as shown in Figure 8; one is a time-based signal process for TOB, and the other is a position-based procedure that is triggered by encoder pulse variation for PBR. The position-based delay can be realized by the read and write process of a memory array in every sampling period according to encoder pulse variation.

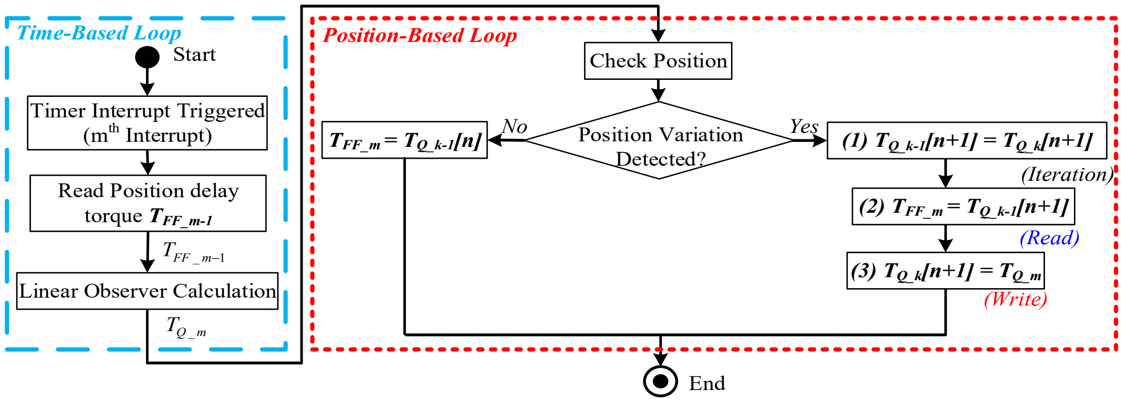

Figure 8. Working flow for PBR-TOB.

This paragraph demonstrates how the position-based delay (by a rotor cycle) is achieved. Let N_{Res}(pulses / turn) be the resolution of an incremental encoder. A learning memory array $T_Q[N_{mem}]$ of size $N_{Mem}(= N_{\text{Res}})$ is utilized to latch the cogging torque information for every position. For example, $T_{Q\_k}[n]$ indicates the latched information for position n at turn k, where $n \in Z[0, N_{\text{Mem}} - 1]$ and $k \in Z[0, \infty]$. With the assumption that the rotor speed $\omega_m > 0$ (*CCW*), once the periodic timer interrupt is triggered at time instance m, the DSP checks if any encoder pulse variation is detected to execute a related position-based procedure. As shown in Figure 9a, if there is no position variation, the memorized data $T_{Q\_k-1}[n]$, corresponding to the cogging torque of position $\boldsymbol{n}$ in the previous turn *k-1*, is set as the feedforward term T_{FF_m} toward the observer. However, as shown in Figure 9b, if the rotor position changes from position n to *n+1*, the position-based delay procedure reads the memory $T_{Q\_k-1}[n+1]$, corresponding to the cogging torque of position *n+1* in the previous turn *k*−*1*, as the feedforward term T_{FF_m}. Simultaneously, T_{Q_m}, the estimated cogging torque of time instance $\boldsymbol{m}$ is latched into the corresponding memory $T_{Q\_k}[N+1]$ as new data for the current turn k.

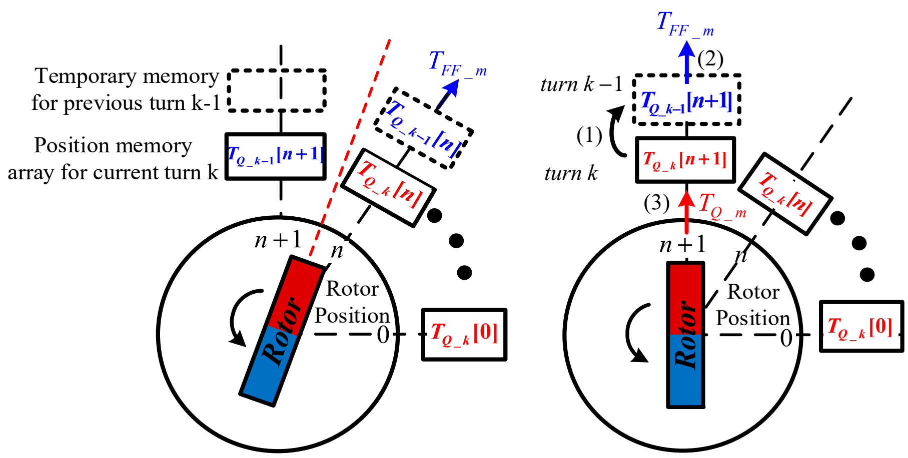

(**a**) (**b**)

Figure 9. Timer interrupt process: (**a**) No position variation is detected; (**b**) Position variation is detected (from n to n + 1).

A simple example with encoder resolution $N_{Mem} = 4$ is demonstrated in Figure 10.

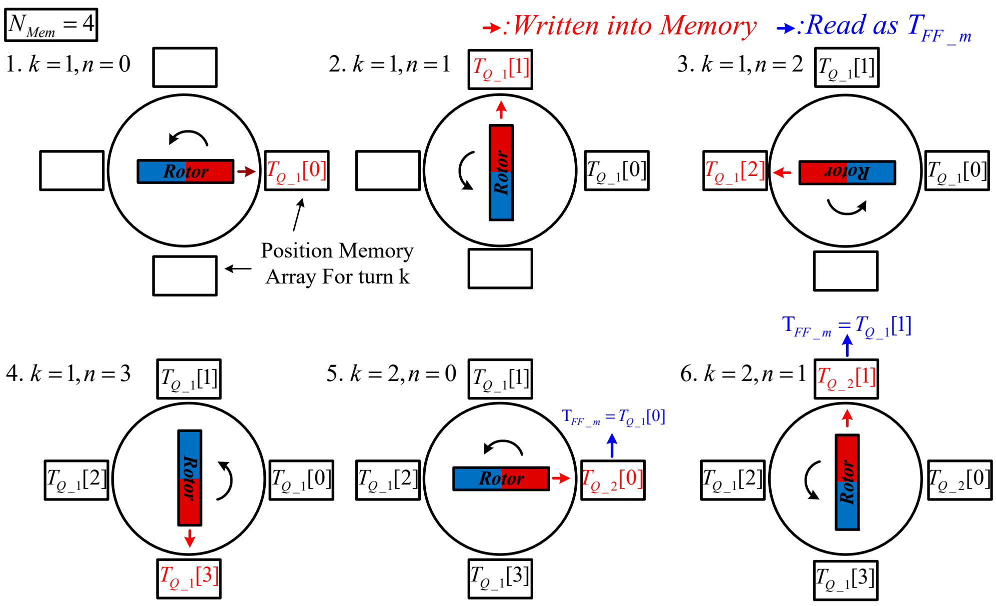

Figure 10. Example for $N_{Mem} = 4$.

However, there are some constraints for the position-based delay process. Since the timer interrupt is triggered under the sample rate $f_S(Hz)$, the frequency of the detected encoder pulse $f_{enc}(Hz)$ can be calculated by the motor speed $\omega_m(rpm)$:

$$f_{enc} = \frac{\omega_m}{60} \times N_{\text{Res}}. \quad (9)$$

As shown in Figure 11, in order to catch all the information into the memory array, according to the Nyquist sampling theorem, the sampling frequency must be higher than two times the encoder frequency.

$$f_S > 2 \times f_{enc} \quad (10)$$

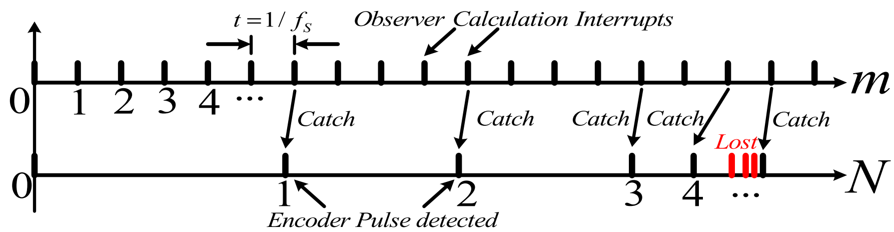

Figure 11. Relation between detected encoder pulse and observer calculation interrupts.

If the conditions mentioned above are satisfied, the cogging torque can be estimated and updated simultaneously, as shown in Figure 12. If the encoder resolution is higher, the resulting observed cogging accuracy is higher.

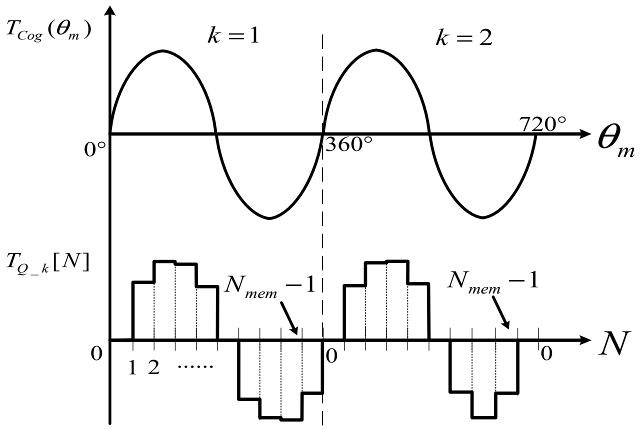

Figure 12. Cogging torque and estimated cogging torque table (no load torque added).

2.4. Torque Compensation Strategy

2.4.1. Online Compensation with Cogging Torque Table Learning Strategy

The online torque compensation strategy is proposed as shown in Figure 13 to provide a closed loop learning process, which updates the estimated cogging torque table as the motor is controlled under a specific speed. Once the cogging torque is well compensated, one can easily observe the torque compensation effect by speed control performance. The processes are listed below.

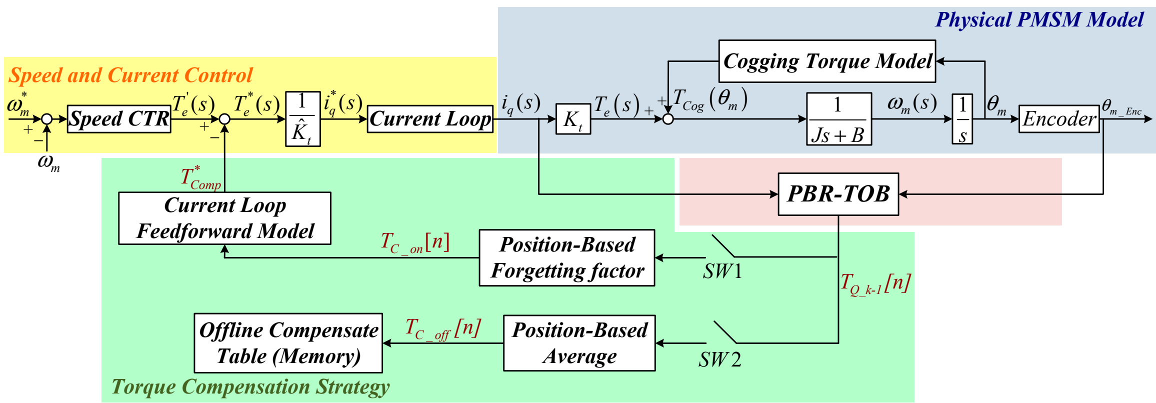

Figure 13. Online compensation with a cogging torque table learning block diagram.

1. Control the motor to a specific speed.
2. After the PBR-TOB operates to steady state, SW1 is switched on to compensate the torque command online.
3. If the compensate effect is not satisfied, one can adjust the cutoff frequency of the learning filter and the bandwidth of PBR-TOB.
4. After the closed loop reaches steady state, SW2 is switched on to get an offline compensate table.

In order to get the best resolution for an offline cogging torque table, the motor is required to control within a specific speed range, which is defined as follows.

1. According to Equations (12) and (13), the motor speed $0 < \omega_m < \frac{30 f_S}{N_{Res}}$ must be satisfied.
2. The lower the speed, the higher the cogging torque resolution.
3. The steady-state speed error is maximum.

Where the steady-state speed error (SSSE) for a certain time interval is defined as:

$$\omega_{m\_SSSE} = \left|Max(\omega_m) - Min(\omega_m)\right|. \tag{11}$$

The online torque compensation strategy is specified as follows. At the first turn, the learning memory array at the last turn $T_{Q\_k-1}[n]$ is used as the initial condition. After the first turn, a forgetting factor W_Q is utilized as Equation (12) to weight the latest observed information $T_{Q\_k-1}[N]$ and the previous compensation information $T_{C\_k-1}[N]$. The observed information in previous turns will be gradually forgotten because of the weighting factor, and the latest observed values would only contribute part of the compensation, such that the noise and uncertainty in each turn can be distributed and reduced. The forgetting factor is chosen to be W_Q= 0.5 in order to balance the weight of the latest and previous data in this paper.

$$\begin{cases} T_{C\_k}[N] = T_{Q\_k-1}[N], \ (first\ compensation\ turn) \\ T_{C\_k}[N] = T_{C\_k-1}[N] \times \left(1 - W_Q\right) + T_{Q\_k-1}[N] \times W_Q (After\ first\ compensation\ turn) \end{cases} \tag{12}$$

When the online compensation strategy reaches the steady state, the offline cogging torque table can be obtained by averaging the observed information T_{Q_k} of l turns at each position such that the noise and uncertainty of each turns can be lowered:

$$T_{C\_Off\_k}[n] = \sum_{k=1}^{k=l} T_{Q\_k}[n]/l. \tag{13}$$

Two advantages of the online strategy are mentioned below. (1) The characteristic of the PBR-TOB is that the cogging torque table will be updated after one rotor turn; in other words, the observation and compensation operate under different rates, and the stability of this structure is relatively high. (2) The initial condition of the learning memory array can be a previous estimated table or a zero array, no matter what the initial condition is, the PBR-TOB alters the table into the shape of the cogging torque. Its potential application is the detection of PM magnetic flux fault.

2.4.2. The Offline Compensation Strategy

After the offline table is obtained, the torque command can be compensated directly by using the offline table, as shown in Figure 14, the online observer structure is no longer needed.

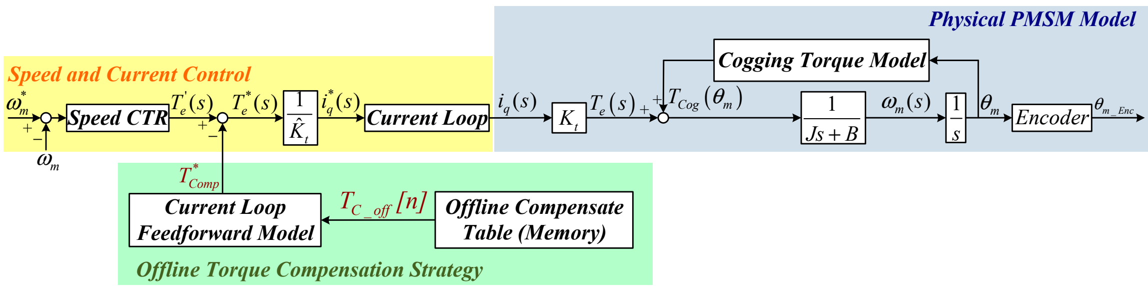

Figure 14. Offline cogging torque compensation block diagram.

In order to compensate the torque command accurately, a current loop feedforward model is proposed, as shown in Figure 15, to overcome the phase lag caused by the current loop. The closed current loop can be simplified as a first-order transfer function with bandwidth $f_c(Hz)$. The torque compensation is in the mechanical angle frame, while the current loop is in the electrical angle frame. In the steady state, the Laplace transform operator "s" can be described as

$$s = j\omega_e = j\frac{N_P}{2}\omega_m, \tag{14}$$

where N_p is the rotor poles number, ω_e and ω_m are the frequencies described under the electrical frame and the mechanical frame, respectively.

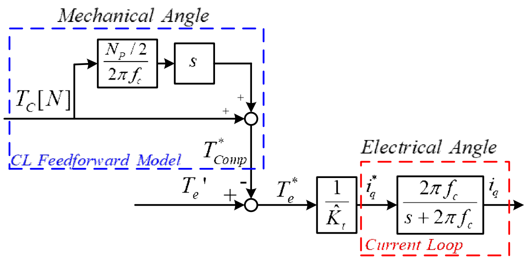

Figure 15. Proposed current loop feedforward model.

Therefore, the feedforward model can be obtained by the inverse of the current loop transfer function; then, t transforms into the mechanical angle frame:

$$\left(\frac{2\pi f_c}{j\omega_e + 2\pi f_c}\right)^{-1} = 1 + \frac{j\omega_e}{2\pi f_c} = 1 + \frac{j\omega_m}{2\pi f_c/(N_P/2)}. \tag{15}$$

3. Experiments

3.1. Hardware Specification and Setup

A PM servomotor is chosen to verify the proposed method along with an encoder of 2000 pulses per cycle, as shown in Figure 16. The specifications of the PMSM are shown in Table 1.

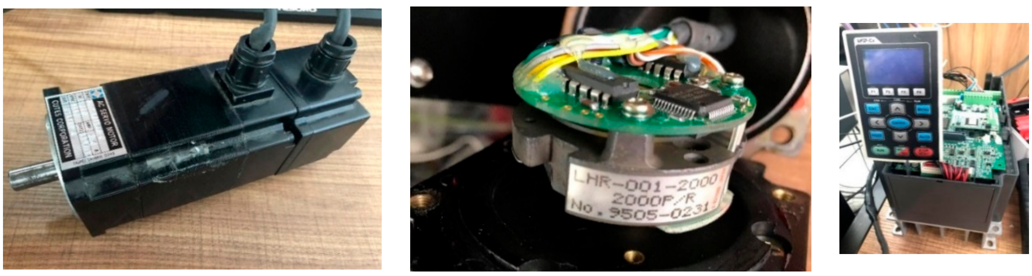

(**a**) AC Servo motor (**b**) ABZ-UVW Encoder (**c**) Driver

Figure 16. PMSM, encoder, and driver for experiment.

Table 1. Servo motor specifications.

PMSM Spec.	Value
Rated Power P_R	0.4 kW
DC Voltage V_{DCBUS}	311 V
Rated Current I_R	2.4 A
Rated Torque T_R	1.1 Nm
Rated Speed ω_R	3000 rpm
Back Electromotive Force (EMF) const. K_e	$19V_{Phase\_RMS}$/krpm
Poles Number N_P	4

A 1.5 kilowatt driver is chosen as shown in Figure 16c, and the specifications of the driver are shown in Table 2.

Table 2. Driver specification.

Driver Spec.	Value
Rated Output Power	1.5 kW
Rated Output Current	8 A(RMS)
Rated Input Current	12 A(RMS)
Rated Input Voltage	200 $\sim$ 240 V $\cdot$ 50/60 Hz
Carrier Frequency	5 $\sim$ 15 kHz

3.2. Experiment Design

One can verify the torque compensation strategy by comparing the steady-state speed error (SSSE) before and after the compensation. As for the HIL experiment, one can easily compare the cogging torque model and its estimation at each position to verify the performance of the proposed observer. Three different experimental conditions were implemented.

- In order to verify the accuracy of the online cogging torque compensation, the procedures are conducted in the following steps:

  1. Control the motor speed to rated speed under no load condition.
  2. Decrease the speed command to find the most appropriate operation speed.
  3. Apply the online torque compensation with the cogging torque learning strategy and compare the SSSE before and after compensation.
  4. Compare the observed cogging torque $\hat{T}_{Cog}(\theta_m)$ with the HIL cogging torque model.

- In order to verify the accuracy of offline cogging torque compensation, the procedures are conducted in the following steps.

  1. Control the motor speed to the most appropriate operation speed and apply the offline torque compensation strategy.
  2. Verify the offline compensation, which can lower the noise compared with online compensation.
  3. Decrease the speed command to lower controllable speed and verify the speed performance.

- As for the rated load condition, the procedures are conducted in the following steps.

  1. Control the motor speed to obtain the most appropriate operational speed under the rated load condition.
  2. Apply the offline torque compensation and compare the SSSE before and after compensation.
  3. Decrease the speed command to lower controllable speed and then verify the speed performance.

3.3. Experiment Results of HIL Emulation

The MR2 HIL device [13], as shown in Figure 17 provides a safe environment for motor drive and control verifications, and it contains a real-time virtual interface of reduced-order motor models, dynamometer, various dynamic load models and power stages. As the control board sends Pulse Width Modulation signals (as control signals) to the six virtual driving gates, the device outputs three-phase current, DC BUS, and position sensors information (as feedback signals) for the control board to drive the motor. The physical motor and power stage mentioned in Section 3.1 can be reconstructed in the HIL system and first-hand verify the control methodology. The cogging torque can be created in any waveform based on the electrical angle, which is chosen to be sinusoid in this verification.

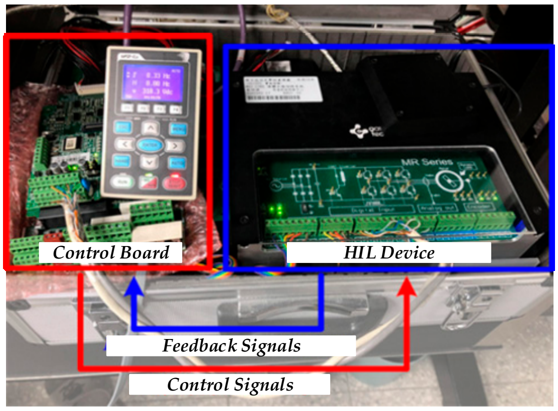

Figure 17. MR2 series Hardware-in-the-Loop (HIL) connects with control board.

Following the experiment design process mentioned in Section 3.2, the most appropriate operation speed is found to be 1 Hz (30 rpm) as depicted in Figure 18a and the SSSE is 47.9255 (rpm). As the online torque compensation is applied, the SSSE drops significantly to 10.7347 (rpm). The offline cogging torque table can be obtained by averaging the observed information for five turns. The comparison between the offline cogging torque table and HIL preset value is shown in Figure 19.

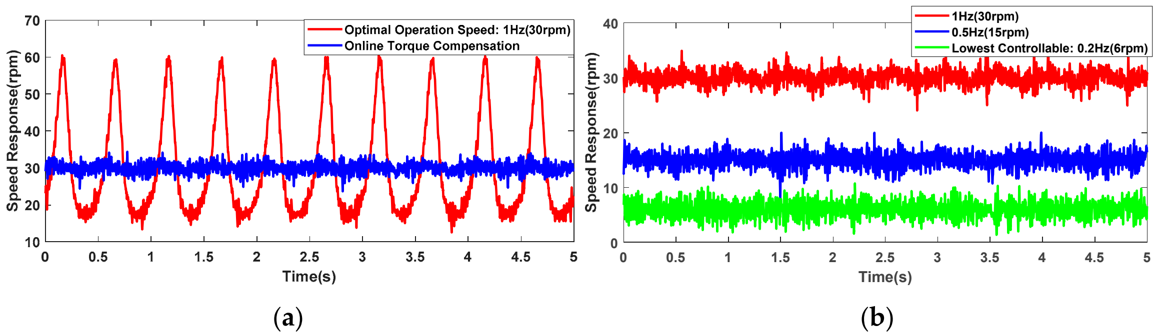

Figure 18. (**a**) Speed comparison before and after online torque compensation; (**b**) Speed response after offline torque compensation.

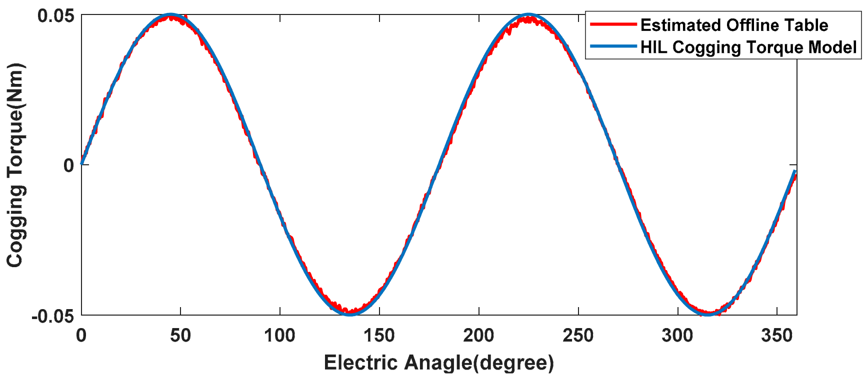

Figure 19. Estimated offline cogging torque table compared with the HIL cogging torque model.

Turn off the online torque compensation and apply the offline torque compensation strategy; then, gradually decrease the speed command. The steady-state speed responses are shown in Figure 18b. The lowest controllable speed can be found at 0.2 Hz (6 rpm). For the SSSE at 1 Hz, 0.5 Hz, and 0.2 Hz, the corresponding steady-state speeds are 10.8306 (rpm), 12.0822 (rpm), and 9.3978 (rpm) respectively. Since the cogging torque model in HIL is perfectly emulated, the SSSE of offline and online compensation are close, and the noise and uncertainty reduction effect cannot be well observed.

Then, we turn off the torque compensation and find the most appropriate operation speed under the rated load. It can be found to be 1 Hz (30 rpm), and the SSSE is 48.9357 (rpm), as shown in Figure 20a. Apply the offline torque compensation strategy, and gradually decrease the speed command. The steady-state speed responses are shown as Figure 20b. The lowest controllable speed can be found at 0.3 Hz (9 rpm). For the SSSE at 1 Hz, 0.5 Hz, and 0.3 Hz are 11.5851 (rpm), 13.8724 (rpm), and 12.8187 (rpm) respectively.

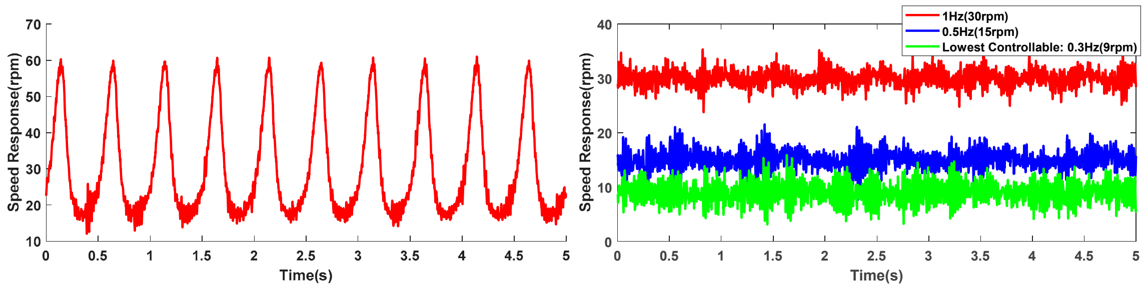

(**a**) (**b**)

Figure 20. Speed response: (**a**) at rated load; (**b**) at rated load after offline torque compensation.

3.4. Experiment Results of Physical Motor Platform

The most appropriate operation speed at no load can be found to be 15 rpm (0.5% rated speed), as shown in Figure 21a, and the SSSE is 31.2344 (rpm). When the online torque compensation strategy is applied, the SSSE drops significantly to 6.3968 (rpm), as shown in Figure 21b. The amplitude of the observed cogging torque is about 0.04 Nm, as shown in Figure 21c. An offset of −0.045 Nm can be observed from the estimated torque, which may be caused by the nonlinear friction of the PMSM and the modeling uncertainty of the observer model. As the online compensate strategy reaches steady state, the offline torque table capture technique is applied. The cogging torque information of five rotary cycles is used to create the offline table. When the offline torque compensate strategy is applied, the SSSE drops significantly to 4.5703 (rpm), as shown in Figure 21d. As can be seen in Figure 21b,d, the resulting SSSE of offline compensation is lower than online compensation, which verifies the noise and uncertainty reduction capability.

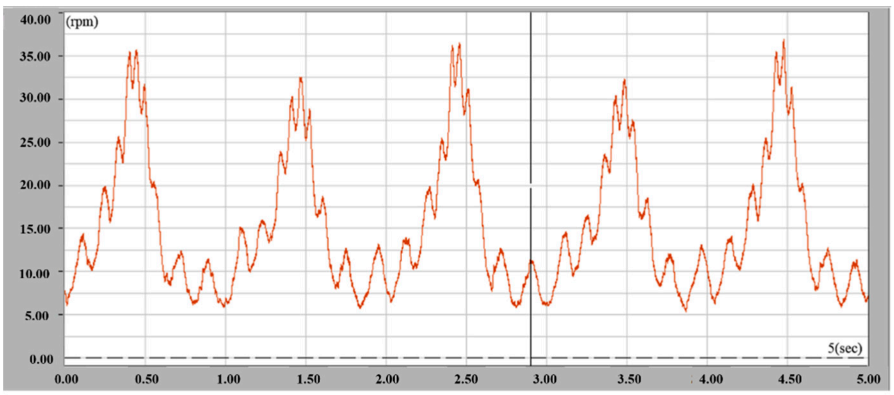

(**a**)

Figure 21. *Cont.*

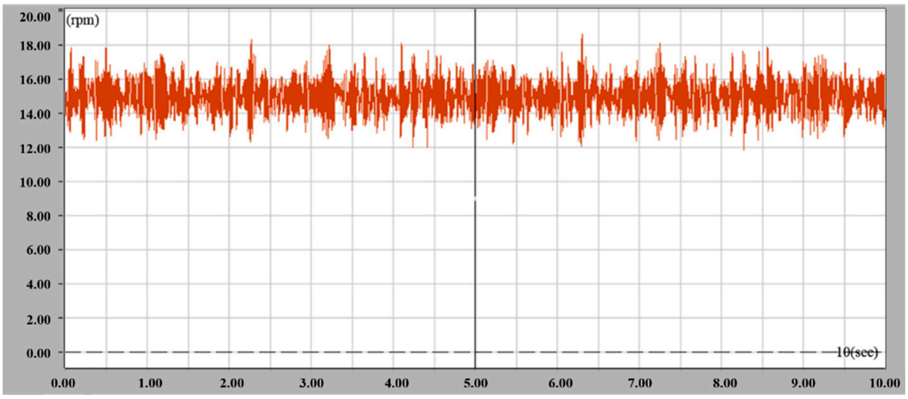

(**b**)

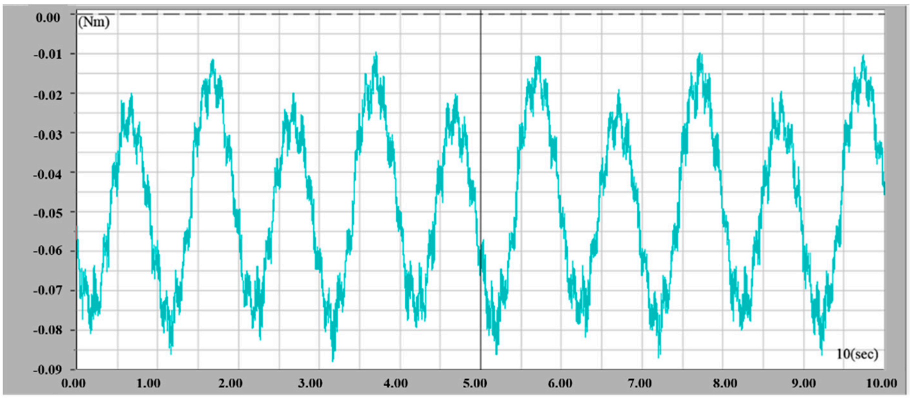

(**c**)

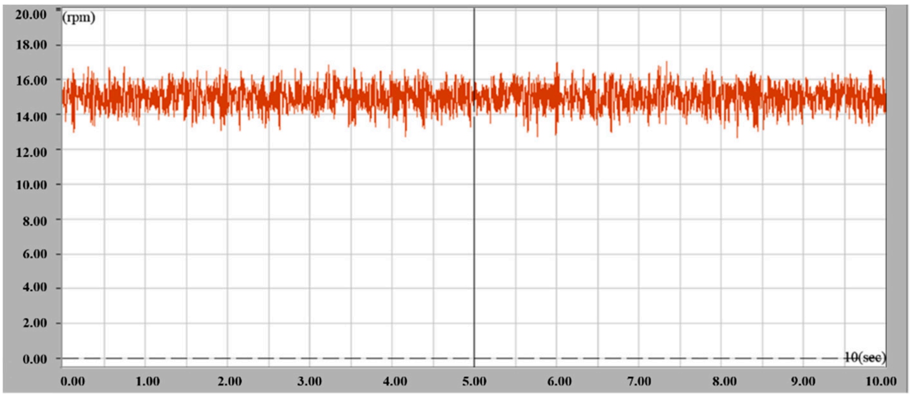

(**d**)

Figure 21. Speed response: (**a**) 15 rpm no load; (**b**) 15 rpm no load by online torque compensation; (**c**) Estimated cogging torque by online torque compensation strategy under 15 rpm no load; (**d**) Offline torque compensates speed response of 15 rpm no load.

In order to create a rated load torque condition, a hysteresis brake is installed as a power measuring device, as shown in Figure 22. The specifications of the hysteresis brake are shown in Table 3.

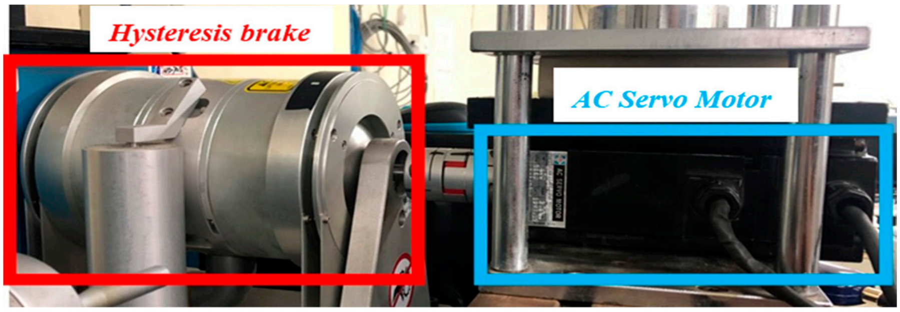

Figure 22. Power meter platform.

Table 3. Power meter specification.

Brake Spec.	Value
Rated Output Torque	6 (Nm)
Max. Speed	25,000 (rpm)
Max. Power	3400 (W)
Poles Number	36

The most appropriate operation speed can be found at about 30 rpm. Since the hysteresis brake is a PM machine, the estimated cogging torque of the PMSM and the brake are combined together. After applying the online torque compensate strategy, the offline cogging torque table can be obtained by averaging the observed information for five turns, as shown in Figure 23a. It can be found that an amplitude of about 0.04 Nm of the PMSM's cogging torque is observed at a low frequency, while an amplitude of about 0.3 Nm of the hysteresis brake's cogging torque is observed at a high frequency. A DC offset of about −0.01 Nm can be observed from the estimated torque, which may be caused by nonlinear friction or the modeling uncertainty of the platform model. Applying a rated load torque of 1.1 Nm, the resulting speed response is shown in Figure 23b where the SSSE is 81.4123 (rpm). After applying the offline torque compensation strategy, the SSSE drops significantly to 8.3834 (rpm), as shown in Figure 23c.

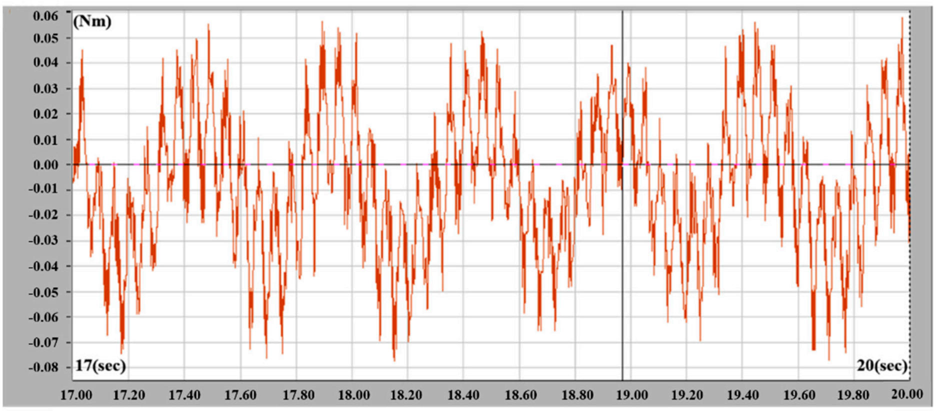

(a)

Figure 23. *Cont.*

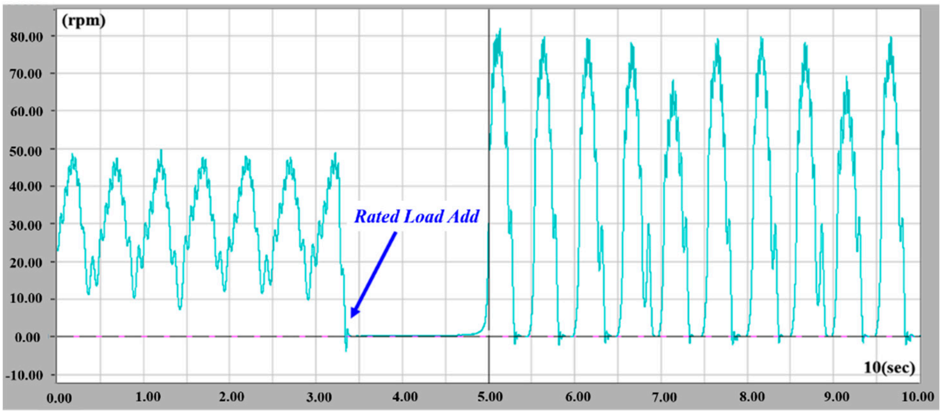

(b)

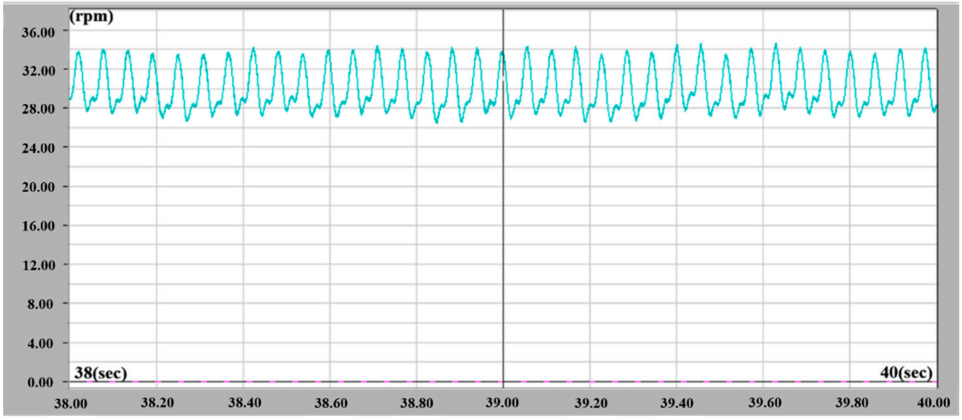

(c)

Figure 23. (**a**) Estimated offline cogging torque of a power meter platform under 30 rpm no load; (**b**) Speed response of the rated step load torque at 30 rpm; (**c**) Speed response with the rated load torque at 30 rpm by offline torque compensation.

4. Conclusions

The contributions of this paper can be summed up below:

(1) Based on the field-oriented control structure, a new observer structure is created to estimate the cogging torque. The proposed observer utilizes the position-based repetitive controller (PBRC) as an internal model in a model reference disturbance observer (MRDOB) to enhance the accuracy of cogging torque estimation.

(2) An incremental encoder is used directly to realize the position-based delay in the PBRC, and a further practical method is introduced to realize the proposed observer with DSP memory array.

(3) Online and offline compensation strategies are proposed, and the position-based forgetting factor and position-based average concept are utilized respectively to reduced noise and uncertainty of the observed information.

(4) The proposed observer and compensation strategies are further verified with HIL emulation and experimental results under no load and rated load conditions. The results show that the cogging torque can be well estimated and the speed ripple can be reduced significantly.

The cogging torque problem occurs not only in PMSM but also in a reluctance motor, such as a synchronous reluctance motor [14], or a switched reluctance motor. Different observer models paired with PBRC can be proposed to minimize the torque and speed ripple with online and offline compensation strategies.

Author Contributions: All authors have read and agree to the published version of the manuscript. Conceptualization, M.-C.T. and C.-J.W.; methodology, M.-C.T. and C.-J.W.; software, L.-J.C. and C.-J.W.; validation, M.-C.T., L.-J.C. and C.-J.W.; formal analysis, M.-C.T., L.-J.C. and C.-J.W.; investigation, M.-C.T. and C.-J.W.; resources, M.-C.T. and L.-J.C.; data curation, L.-J.C. and C.-J.W.; writing—original draft preparation, C.-J.W.; writing—review and editing, M.-C.T. and L.-J.C., C.-J.W.; visualization, C.-J.W.; supervision, M.-C.T. and L.-J.C.; project administration, M.-C.T. All authors have read and agreed to the published version of the manuscript.

Funding: This research received no external funding.

Acknowledgments: This work is supported by the DELTA ELECTRONICS, INC, and the Ministry of Science and Technology (MOST), Taiwan, under grants numbers MOST 106-2221-E-006-251-MY3 and MOST 108-2622-8-006-014.

Conflicts of Interest: The authors declare no conflict of interest.

References

1. Studer, C.; Keyhani, A.; Sebastian, T.; Murthy, S.K. Study of cogging torque in permanent magnet machines. In Proceedings of the IAS 97. Conference Record of the 1997 IEEE Industry Applications Conference Thirty-Second IAS Annual Meeting, New Orleans, LA, USA, 5–9 October 1997; Volume 1, pp. 42–49.
2. Setiabudy, R.; Wahab, H.; Putra, Y.S. Reduction of cogging torque on brushless direct current motor with segmentation of magnet permanent. In Proceedings of the2017 4th International Conference on Information Technology, Computer, and Electrical Engineering (ICITACEE), Semarang, Indonesia, 18–19 October 2017; pp. 81–86.
3. Wahab, H.; Setiabudy, R.; Rahardjo, A. Cogging torque reduction by modifying stator teeth and permanent magnet shape on a surface mounted PMSG. In Proceedings of the 2017 International Seminar on Intelligent Technology and Its Applications (ISITIA), Surabaya, Indonesia, 28–29 August 2017; pp. 227–232.
4. Ueda, Y.; Takahashi, H.; Ogawa, A.; Akiba, T.; Yoshida, M. Cogging-Torque Reduction of Transverse-Flux Motor by Skewing Stator Poles. *IEEE Trans. Magn.* **2016**, *52*, 1–4. [CrossRef]
5. Ge, X.; Zhu, Z.Q.; Kemp, G.; Moule, D.; Williams, C. Optimal Step-Skew Methods for Cogging Torque Reduction Accounting for Three-Dimensional Effect of Interior Permanent Magnet Machines. *IEEE Trans. Energy Convers.* **2017**, *32*, 222–232. [CrossRef]
6. Ellis, G. *Observers in Control Systems: A Practical Guide*; Academic Press: Cambridge, MA, USA, 2002.
7. Li, P.Y. Internal Model Principle, Lecture of Advanced Control System Design. 2016. Available online: http://www.me.umn.edu/courses/me8281/Old/IMP-repetitive.pdf (accessed on 17 August 2018).
8. Żak, S.H. The Internal Model Principle, Lecture of Feedback System Analysis and Design. 2016. Available online: https://engineering.purdue.edu/~{}zak/ECE_382-2014/hand_3.pdf (accessed on 13 August 2018).
9. Chen, C.L.; Tsai, M.C. Position-Dependent Repetitive Control for Speed Ripple Reduction of Ultrasonic Motor. *IFAC Proc. Vol.* **2014**, *47*, 1754–1759. [CrossRef]
10. Hara, S.; Yamamoto, Y.; Omata, T.; Nakano, M. Repetitive Control-System—A New Type Servo System for Periodic Exogenous Signals. *IEEE Trans. Autom. Control* **1988**, *33*, 659–668. [CrossRef]
11. Tsai, M.C.; Yao, W.S. Design of a plug-in type repetitive controller for periodic inputs. *IEEE Trans. Control Syst. Technol.* **2002**, *10*, 547–555. [CrossRef]
12. Tsai, M.C.; Yao, W.S. Implementation of Repetitive Controller for Rejection of Position-based Periodic Disturbances. *Control Eng. Prac.* **2013**, *21*, 1226–1237.
13. Gathertech Corp. Lmt. MR2 HIL User Manual. Available online: https://www.gathertech.net/en-us-hil-product (accessed on 18 December 2019).
14. Yousefi-Talouki, A.; Pellegrino, G. Sensorless direct flux vector control of synchronous reluctance motor drives in a wide speed range including standstill. In Proceedings of the 2016 XXII International Conference on Electrical Machines (ICEM), Lausanne, Switzerland, 4–7 September 2016; pp. 1167–1173.